Supporting information for

Insight into the Oriented Growth of Surface-Attached Metal-Organic Frameworks: Surface Functionality, Deposition Temperature, and First Layer Order

Jin-Liang Zhuang,[†,‡,§] Martin Kind,[†] Claudia M. Grytz,[†] Frederic Farr,[†] Martin Diefenbach,[†] Samat Tussupbayev,[†] Max C. Holthausen,[†] and Andreas Terfort*[,†]

[†]Institute of Inorganic and Analytical Chemistry, University of Frankfurt, Max-von-Laue-Strasse 7, 60438 Frankfurt, Germany

[‡]School of Chemistry and Materials, Guizhou Normal University, Guiyang, 550001, P. R. China

[§]State Key Laboratory of Physical Chemistry of Solid Surfaces, Xiamen University, Xiamen 361005, P. R. China

Experimental Section

Reagents:

$Cu(NO_3)_2 \cdot 3H_2O$ (ABCR GmbH), $Cu_2(OAc)_4 \cdot 2H_2O$ (Carl Roth GmbH), tetrafluoro-benzene-1,4-dicarboxylic acid (H_2F_4bdc, Apollo Scientific Limited), 1,4-diazadicyclo[2.2.2]octane (dabco, ABCR GmbH), CD_3COOD (Eurisotop), D_2O (Eurisotop), 1-hexadecanethiol (HDT, Fluka), absolute ethanol (Sigma-Aldrich), trifluoroacetic acid (TFA, Acros Organics).

SAM-functionalized substrates:

The Au substrates were manufactured by electron-beam evaporation of 5 nm of Cr and 100 nm of Au onto four inch Si wafers with (100) orientation. When these films could not be used immediately, they were cleaned by immersion into a 10 mM 1-hexadecanethiol (HDT) solution in ethanol for 2 hours followed by a 2 min treatment in H_2 plasma.[1] The clean gold substrates were immersed for 48 h either in a 0.1 mM (4-(4-(4-pyridyl)phenyl)phenyl)methanethiol (PPP1, synthesized according to ref [2]) solution in ethanol or in a half saturated solution of 4'-(mercaptomethyl)- terphenyl-4-carboxylic acid (MTCA, synthesized according to ref. [3], was sonicated in ethanol to obtain a saturated solution, which

was, after filtration, diluted with an equal amount of ethanol to avoid precipitation of the MTCA). Since MTCA usually forms bilayers on gold because of hydrogen bond formation, trifluoroacetic acid (TFA) was used to break the hydrogen bonds and thus to remove the second layer. For this, the MTCA-covered substrates were rinsed with ethanol, and then sonicated in a TFA solution (2 drops of TFA in 20 mL ethanol) for 5 min. After rinsing with ethanol and drying in a stream of N_2, the substrate was treated in a vacuum chamber at 5 mbar for 30 min to remove the TFA. All substrates were washed with ethanol before the step-by-step growth.

Synthesis of $Cu_2(CD_3COO)_4 \cdot xD_2O$:

CD_3COOD (2.0 g, 0.03 mol) and $Cu_2(OH)_2CO_3$ (1.0 g, 4.5 mmol) were dissolved in D_2O (25.6 g, 1.28 mol). The mixture was refluxed at 120 °C (bath temp.) under N_2 atmosphere for 48 h. The dark blue solution was evaporated under vacuum and $Cu_2(CD_3COO)_4 \cdot 2D_2O$ (1.69 g) was obtained.

Synthesis of bulk $[Cu_2(F_4bdc)_2(dabco)]$:

The synthesis of $[Cu_2(F_4bdc)_2(dabco)]$ was similar to the synthesis of $[Zn_2(F_4bdc)_2(dabco)]$ as reported previously:[4] $Cu(NO_3)_2 \cdot 3H_2O$ (193 mg, 0.80 mmol) and H_2F_4bdc (190 mg, 0.80 mmol) were dissolved in methanol (10 mL). The mixture was dropped into a solution of dabco (45 mg, 0.4 mmol) in DMF (2.5 mL) under stirring. The slurry was further stirring for 1 h and then the precipitate was filtered off. The resulting clear blue solution was sealed in a glass vial and heated at 85 °C overnight. Green crystals were obtained and washed with DMF and methanol. The crude product was further purified by immersing in methanol solution overnight and dried under vacuum. Finally, $[Cu_2(F_4bdc)_2(dabco)]$ dark green crystals (0.174 g) were obtained.

Step-wise layer-by-layer growth of $[Cu_2(F_4bdc)_2(dabco)]$ film on surfaces:

Layer-by-layer deposition was performed in a home-made temperature controllable glass cell. The functionalized substrates were alternatingly immersed into a solution of (deuterated) copper acetate in ethanol (1 mM) for 20 min and in an equimolar H_2F_4bdc/dabco mixture (0.1 mM each) for 40 min. Between each step, the substrate was immersed into fresh ethanol for 5 min twice.

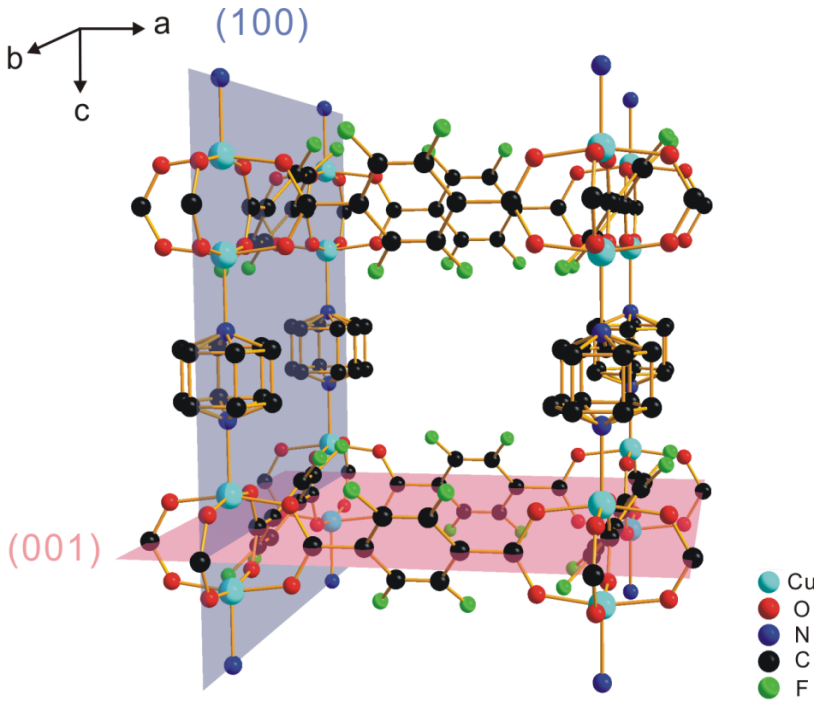

Figure S1. The unit cell of $[Cu_2(F_4bdc)_2(dabco)]$ shows two principal growth directions that are either preferred on pyridyl- ([001]) or carboxylate- ([100]) terminated SAMs. Please observe that the dabco ligands are represented as disordered.

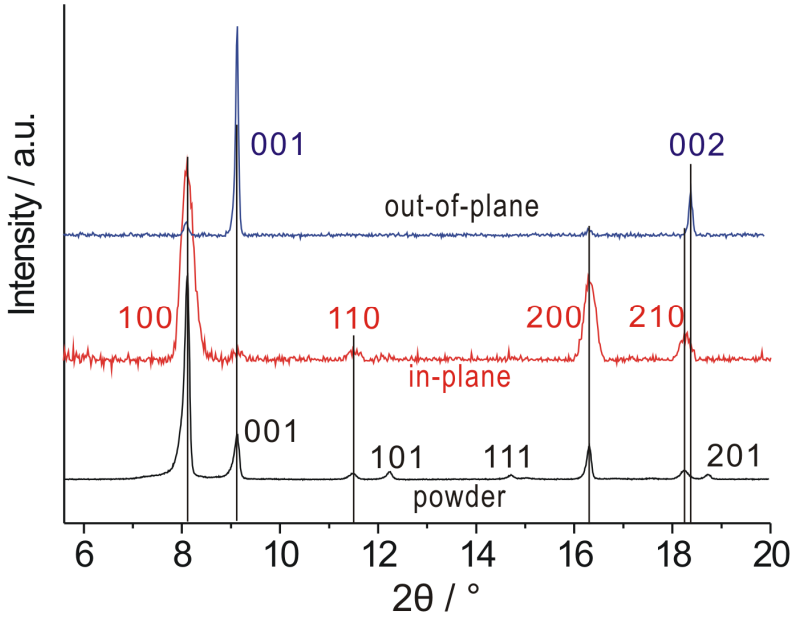

Figure S2. Out-of-plane and in-plane XRD data of $[Cu_2(F_4bdc)_2(dabco)]$ grown on a PPP1 surface (50 cycles) at 60 °C. The XRD powder pattern of $[Cu_2(F_4bdc)_2(dabco)]$ is also shown for diffraction peak assignment.

Characterization

SEM images were recorded using a JEOL JSM 7001F scanning electron microscope. Powder X-ray diffraction patterns were collected between 2θ = 2° and 80°, on a STOE theta-theta diffractometer using Cu Kα1 (1.5418 Å) radiation and a linear position-sensitive detector. The surface X-ray diffraction (SXRD) measurements were performed in theta/theta mode, with a step width of 0.02°, and a scan rate 100s/step for thin film sample. AFM measurements were performed on a NanoScope Dimension^{TM} 3100 atomic force microscope in tapping mode. FT-IR spectra were recorded with a NICOLET 6700 Fourier Transform Infrared Reflection-Absorption Spectrometer. For bulk substances a diamond ATR cell was used, for thin films on reflective substrates (gold) a modified smart SAGA unit providing an incidence angle of 80° was utilized. SAMs of perdeuterated hexadecanethiol ($C_{16}D_{33}SH$) on gold were used as background samples for thin film FT-IR measurement.

IR Calculation and Band Assignment

Infrared vibrational band assignment of the diaqua-tetrakis-μ-acetato-dicopper complex

The vibrational bands of $Cu_2(CH_3COO)_4 \cdot 2H_2O$ and $Cu_2(CD_3COO)_4 \cdot 2D_2O$ were assigned by comparison of experimental FT-IR spectra of both compounds to their theoretical counterparts which were calculated using density functional theory (DFT). The calculation outputs were also used to analyze the direction of the vibrational modes' transition dipole moments (TDMs) relative to the Cu-Cu axes of the complexes.

Theoretical vibrational spectra of the non-deuterated and the deuterated copper complexes were calculated with the Gaussian 09 program package[5], employing the B3LYP functional and the def2-SVP basis set. To account for the open shell electron configuration of the two copper atoms in the complexes, the broken symmetry ansatz was used; an unrestricted wavefunction was generated using the "guess=mix" option in Gaussian 09.

A common scaling factor of 0.973 for both calculated spectra was obtained by averaging the ratios of the experimental vs. theoretical wavenumber positions of bands **6** (non-deuterated copper acetate) and **7** (deuterated copper acetate), respectively.

In figures S2 and S3, the experimental and scaled calculated spectra of the copper complexes are

displayed. The assignment, TDM orientations and wavenumbers of the most important vibrational modes of both copper complexes are listed in tables S1 and S2.

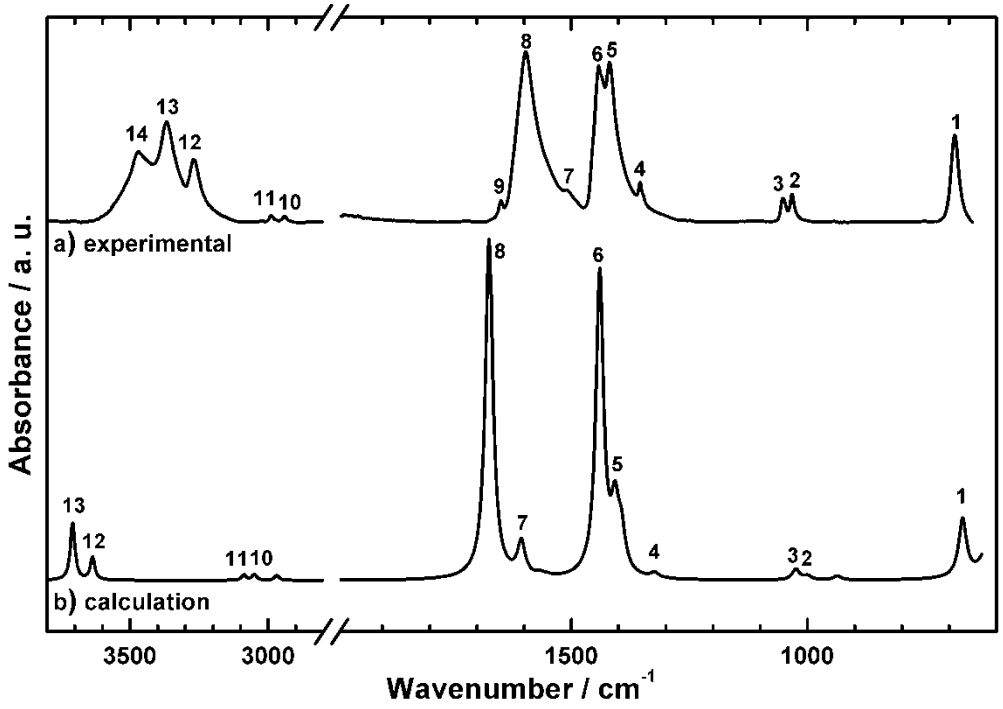

Figure S3. Infrared spectra of the $Cu_2(CH_3COO)_4 \cdot 2H_2O$ complex. a) Experimental spectrum of the neat substance, recorded with an attenuated total reflection unit, b) calculated spectrum using broken symmetry density functional theory. For assignment of the bands, see table S1.

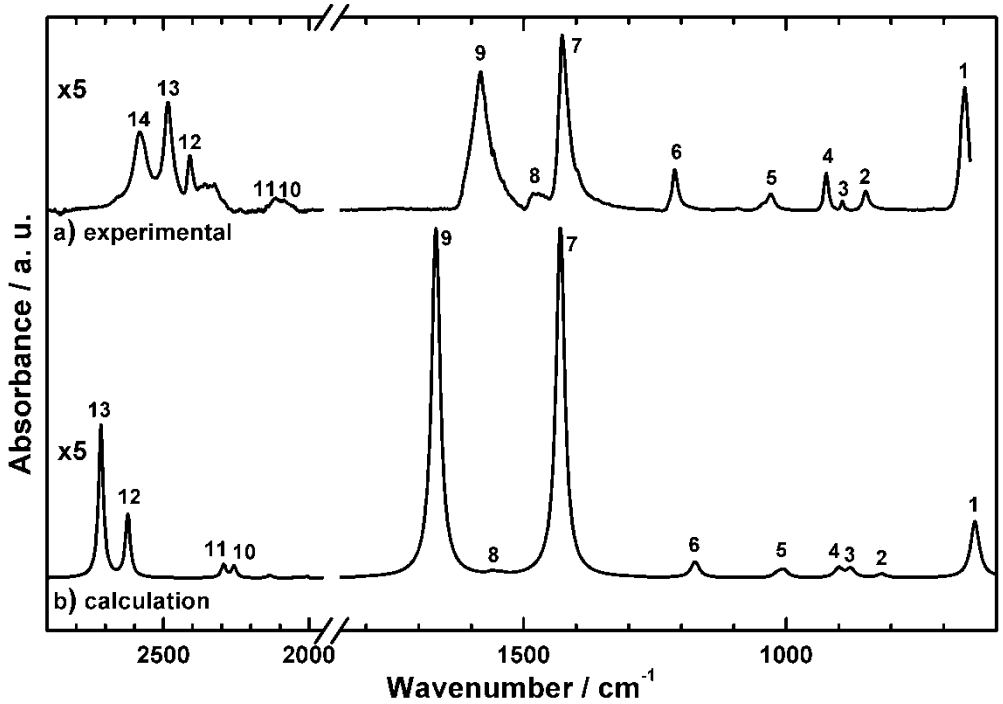

Figure S4. Infrared spectra of the $Cu_2(CD_3COO)_4 \cdot 2D_2O$ complex. a) Experimental spectrum of the neat substance, recorded

with an attenuated total reflection unit, b) calculated spectrum using broken symmetry density functional theory. For assignment of the bands, see table S2.

Table S1. Assignment of vibrational modes of the $Cu_2(CH_3COO)_4 \cdot 2H_2O$ complex.

Experimental (Exp.) and calculated (Calc.) wavenumbers are given in cm^{-1}. Calculated frequencies are scaled by a factor of 0.973. For some bands, the orientation of the transition dipole moment (TDM) with respect to the Cu-Cu axis is given (||: parallel, _|_: perpendicular).

No.	Vibrational Mode*	TDM	Exp.**	Lit.[6]	Calc.
1	ν CC, δ_{bend} CO_2	_|_	688 s	690	671
2	$\delta_{bend, as}$ CH_3	||	1032 m	1032	999
3	δ_{rock} CH_3	_|_	1051 m	1053	1024
4	$\delta_{bend, s}$ CH_3		1353 m	1356	1323
5	$\delta_{bend, as}$ CH_3		1419 vs	1425	1401
6	ν_s CO_2, ν CC, $\delta_{bend, as}$ CH_3	_|_	1442 vs	1460	1440
7	δ_{bend} OH_2		1510 m (sh)		1606
8	ν_{as} CO_2, δ_{rock} CH_3	||	1585 vs	1605	1674
9			1648 w		***
10	ν_{as} CH_3	_|_	2941 w		3051
11	ν_{as} CH_3	||	2988 w		3088
12	ν_s H_2O		3272 m		3636
13	ν_{as} H_2O		3368 s		3708
14	ν H_2O		3468 m		***

*) ν: stretch mode, δ: deformation, bend: bending, as: asymmetric, rock: rocking, s: symmetric

**) vs: very strong, s: strong, m: medium, w: weak, sh: shoulder

***) does not appear in the calculated spectrum

Table S2. Assignment of vibrational modes of the $Cu_2(CD_3COO)_4 \cdot 2D_2O$ complex.

Experimental (Exp.) and calculated (Calc.) wavenumbers are given in cm^{-1}. Calculated frequencies are scaled by a factor of 0.973. For some bands, the orientation of the transition dipole moment (TDM) with respect to the Cu-Cu axis is given (||: parallel, _|_: perpendicular).

No.	Vibrational Mode*	TDM	Exp.**	Calc.
1	ν CC, δ_{bend} CO_2	_|_	661 vs	641
2	δ_{rock} CO_2, δ_{rock} CD_3	||	850 w	818
3	δ_{bend} CD_3, δ_{bend} CO_2	_|_	893 w	877
4	δ_{rock} CD_3	_|_	924 m	900
5	$\delta_{bend, as}$ CD_3	||	1029 w	1004
6	δ_{bend} OD_2	_|_	1213 m	1173
7	ν_s CO_2, ν CC, $\delta_{bend, as}$ CD_3	_|_	1428 vs	1430
8	ν_{as} CO_2, δ CC	_|_	1479 w	1560
9	ν_{as} CO_2, δ CC	||	1584 vs	1667
10	ν_{as} CD_3	_|_	2086 w	2257
11	ν_{as} CD_3	||	2113 w	2293
12	ν_s D_2O		2408 w	2623
13	ν_{as} D_2O		2485 m	2715
14	ν D_2O		2580 m	***

*) ν: stretch mode, δ: deformation, bend: bending, rock: rocking, as: asymmetric, s: symmetric

**) vs: very strong, s: strong, m: medium, w: weak

***) does not appear in the calculated spectrum

The experimental spectra of both complexes exhibit additional water bands at 3468 cm^{-1} (H_2O, band **14**) and 2580 cm^{-1} (D_2O, band **14**), respectively, which are attributed to crystallization water in addition to the coordinated water molecules (bands **12** and **13** in the spectra of both complexes). A weak signal (1648 cm^{-1}, band **9**) in the spectrum of $Cu_2(CH_3COO)_4 \cdot 2H_2O$ suggests a slight contamination, probably free acetate. A number of bands are shifted due to the isotope effect, e.g. the vibrational modes involving OH/OD stretching (bands **12**, **13**, **14** in the spectra of both complexes), OH/OD bending (band **7**, non-deuterated complex; band **6**, deuterated complex) CH/CD stretching (bands **10** and **11** in the spectra of both complexes) or CH/CD bending and rocking (e.g. band **3**, non-deuterated complex; band **4**, deuterated complex). The critical band that brought us to perform most experiments with the deuterated copper complex is located at 1419 cm^{-1} in the spectrum of the non-deuterated complex (band **5**). This band almost overlaps with the symmetric CO_2 stretch mode (band **6**). Since band **5** is due to a couple of CH bending modes with different TDM orientations, it can hamper the evaluation of the orientation of the Cu-Cu axis with respect to the substrate surface.

To make sure that no other signals from the ligands hamper the determination of the orientation, bulk IR spectra of the free ligands, in the case of F_4bdc in the form of its sodium salt, were recorded (Figure S4). As can be seen, the IR spectrum of the MOF is dominated by the spectral features of the F_4bdc anion. Overlaps of the carboxylate vibrations with either other features of the F_4bdc ligand or by the dabco ligand could not be observed.

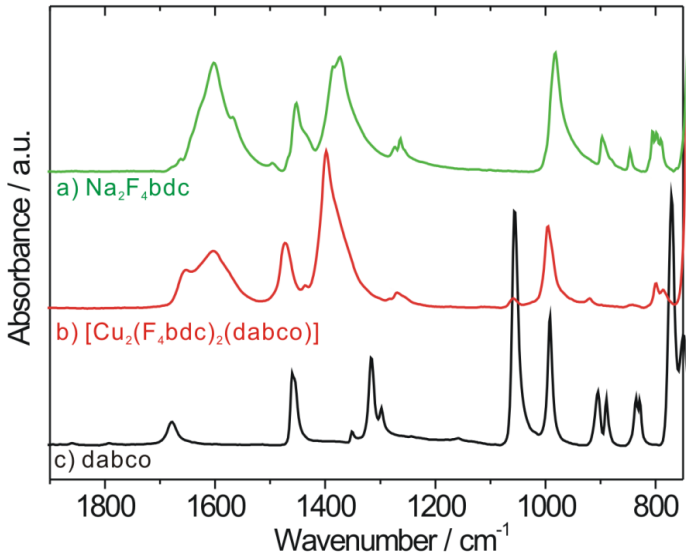

Figure S5. Bulk Fourier transform infrared spectra of the $[Cu_2(F_4bdc)_2(dabco)]$ MOF and its ligands, recorded with an ATR unit. a) Disodium tetrafluorobenzene-1,4-dicarboxylate (Na_2F_4bdc) b) $[Cu_2(F_4bdc)_2(dabco)]$ synthesized by the solvothermal method, and c) 1,4-diazadicyclo[2.2.2]octane (dabco).

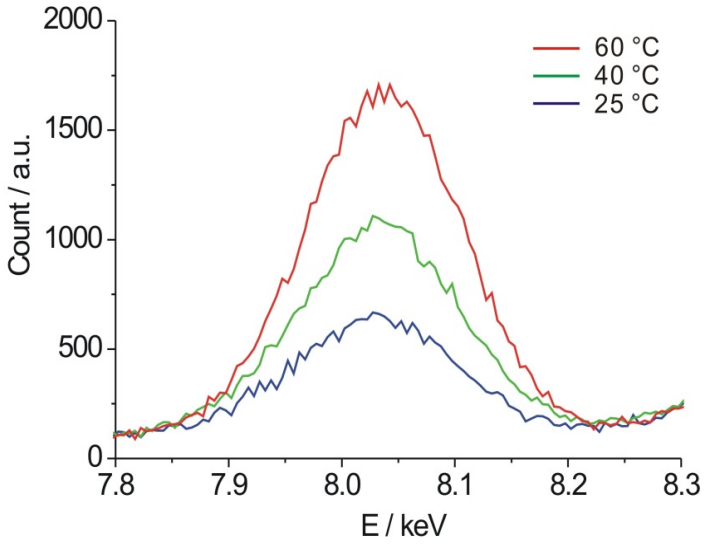

Figure S6. Total external reflection X-ray fluorescence (TXRF) spectra of $Cu_2(CH_3COO)_4{\cdot}2H_2O$ deposited from ethanolic solution (1 mM, 20 min) onto PPP1 surfaces at various temperatures. The intensity correlates with the intensity of the respective carboxylate vibrational bands in the IRRA spectra, ruling out the possibility of decomposition/reorganization of the Cu_2 unit at the surface.

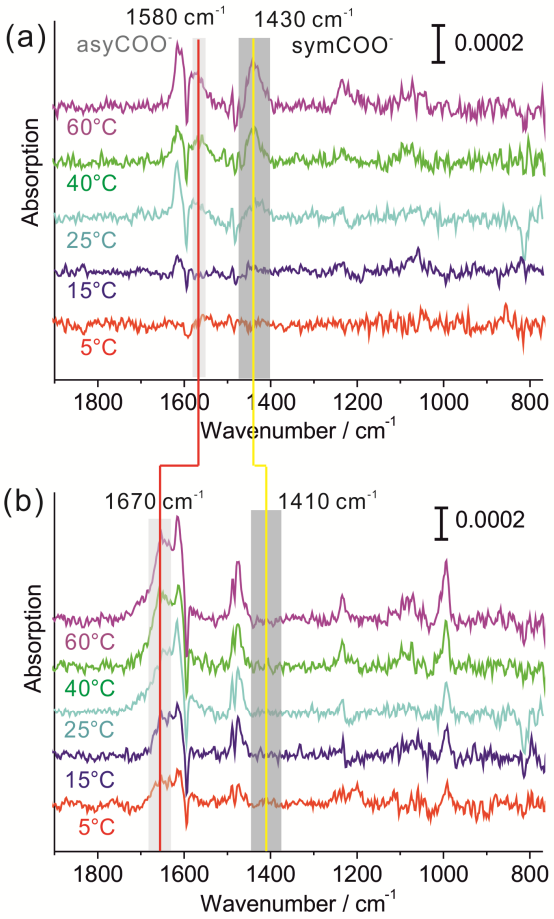

Figure S7. The IRRA spectra of the deposits on PPP1 SAMs after half cycle (a) and first cycle (b) as shown in Figure 3, here after subtraction of the PPP1 background. This subtraction permitted the better isolation of the carboxylate vibrations, permitting the quantitative evaluation. The negative peaks at 1600 cm^{-1} and 1480 cm^{-1} indicate the shifts of the respective PPP1 signals due to coordination. The yellow and red vertical lines signify the shift of the carboxylate signals due to the replacement of the acetate ligands by the F4bdc ligands (the symmetric vibration of the F4bdc carboxylate is not visible in the lower panel because of their high orientational order, see text).

Quantum-chemical study

The quantum-chemical study of the metal-organic frameworks on the surface was performed using model paddle wheels (cf. Figure S7), where the F_4bdc linker molecules were substituted by trifluoroacetic acid (TFA). The structures were optimized at the PBE/def2-SVP[7,8] level using the Gaussian 09 program package.[5] The following single point calculations were performed with the ORCA 2.8 program package[9] employing the B3LYP-D hybrid functional,[10-12] which includes dispersion correction,[13] in conjunction with the larger def2-TZVP basis set.[8] The 10 core electrons of copper were replaced by the quasi-relativistic effective core potential SDD [14] for copper complemented by the triple-ζ quality valence basis set.[15] The broken symmetry ansatz was also used in ORCA 2.8 by including the "brokensym" option in calculations. Solvent effects were taken into account implicitly using the COSMO solvation model.[16]

Commencing with structure **A,** the Cu–Cu vector is oriented parallel to the surface (cf. Figure S7). Dissociation of the apical dabco ligand consumes about $24\,\mathrm{kcal\,mol^{-1}}$ and affords structure **B.** The relative stability of the intermediate **B** can be used as a rough estimate for the reorientation energy barrier. The substantial tilt of the Cu–Cu vector in structure **C** is induced by a shift of the surface acetate linker from the basal bidentate η^2 coordination towards the apical (η^1) position, concomitant with re-coordination of dabco at the opposite apical Cu site. The subsequent proton shift from the (more acidic) TFA molecule to the surface-bound carboxylate results in structure **D,** leading to a complete reorientation of the Cu_2 unit. The sequence shown in Figure S7 may be interpreted in terms of a fast equilibrium between a parallel orientation of the Cu_2 unit to a perpendicular one. The relative energy of structure **B** is roughly of the order of the energy regime available at room temperature, and temperatures above room temperature will accelerate the reaction sequence.

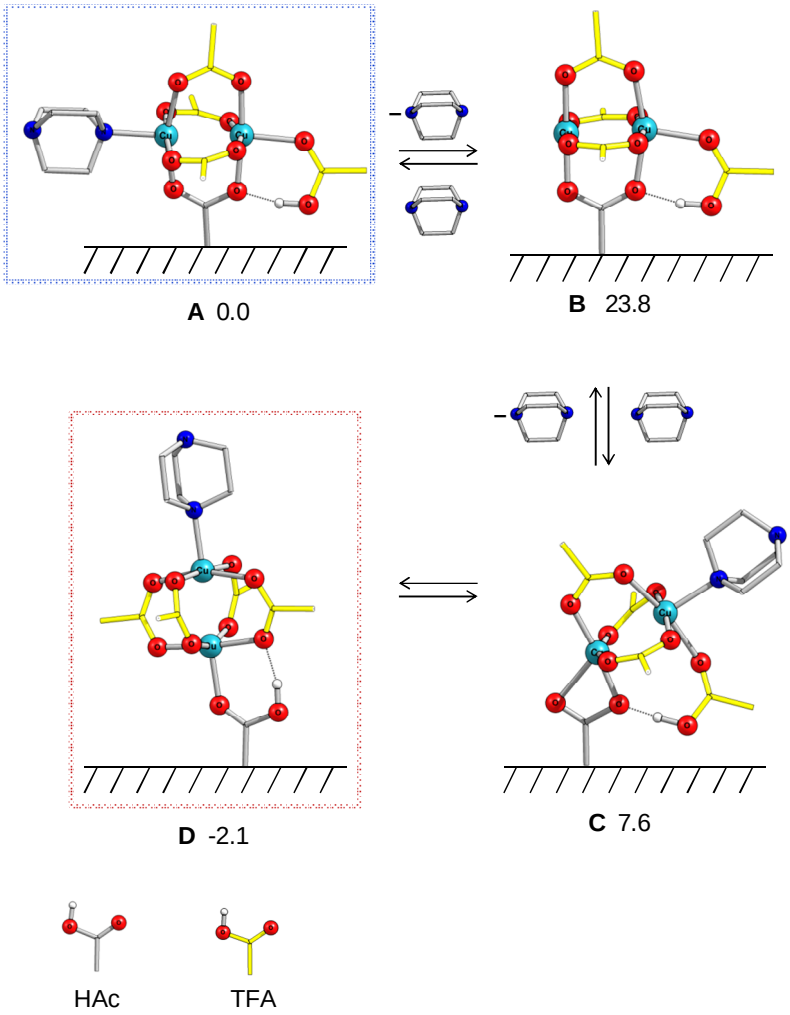

Figure S8. Mechanistic model scenario of the reorientation of the Cu_2 paddle wheels on the surface upon addition of the carboxylate ligand. B3LYP-D(methanol)/def2-TZVP(PP)//PBE/def2-SVP relative enthalpies of formation $\Delta_f H_{298}$ are given in kcal mol^{-1}.

Evaluation of orientational composition of the SURMOFs

a) From SXRD data

Since in the SXRD only diffraction peaks with (100) and (001) index could be observed, the following evaluation procedure neglects all the other reflections observable in the bulk powder XRD. In the powder sample, completely disoriented alignment was expected, which means that the proportions $X_{(001)}$ and $X_{(100)}$ of the [001]- and [100]-oriented crystals, respectively, are equal:

$$X_{(001)} = X_{(100)} \qquad \text{Eq. 1}$$

Since the intensities $I_{(xyz)}$ are not the same, an intensity factor f_{XRD} can be introduced

$f_{XRD} = (I_{(100)} * X_{(001)}) / (I_{(001)} * X_{(100)}) = I_{(100)} / I_{(001)}$ Eq. 2

This permits also to determine the ratio of the proportions of (001)- and (100)-oriented crystals ($\chi_{(001)}$ and $\chi_{(100)}$, respectively) on the surface from the intensities in the SXRD ($i_{(001)}$ and $i_{(100)}$):

$f_{XRD} = (i_{(100)} * \chi_{(001)}) / (i_{(001)} * \chi_{(100)})$ Eq. 3

Since in the SURMOFs only the orientations (100) and (001) were found, the proportions of these must sum up to unity:

$\chi_{(001)} + \chi_{(100)} = 1$ Eq. 4

Solving Eq. 3 for $\chi_{(100)}$ and insertion into Eq. 4 results in

$\chi_{(001)} + (\chi_{(001)} * f_{XRD} * i_{(001)}) / i_{(100)} = 1$ Eq. 5

which after replacement of f_{XRD} (Eq. 2) is used in its reformed form:

$$\chi_{(100)} = \frac{1}{1 + \frac{i_{(001)}}{i_{(100)}} \times \frac{X_{(100)}}{X_{(001)}}}$$ Eq. 6

b) From IRRAS data

The evaluation scheme follows the one for the XRD data. The significant difference is that in the bulk, the statistic contribution of the **A**symmetric and the **S**ymmetric vibration of the carboxylate group are the same, ($X_A = X_S$), permitting the determination of a sensitivity factor f_{IR}:

$f_{IR} = (I_A * X_S) / (I_S * X_A) = I_A / I_S$ Eq. 7

with I_A and I_S being the signal intensities determined in the bulk. On the other hand, the contributions of the vibrations are not equal at the surface due to the surface selection rules (Figure S8): When the clusters are oriented with their Cu-Cu axis perpendicular to the surface (as is the case in [001] oriented crystals), all four carboxylate groups contribute to the signal of the **A**symmetric vibration, while in the cluster with the axis parallel to the surface (as in case of the [100] oriented crystals) only two carboxylate groups contribute to the **S**ymmetric signal, resulting in the intensities i_A and i_S, respectively.

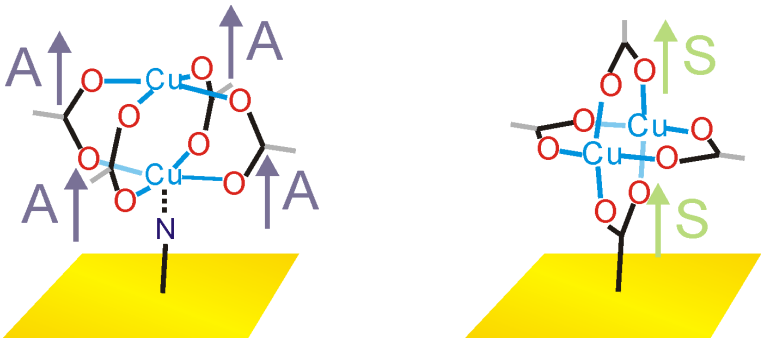

Figure S9. Illustration of the contribution of the carboxylate groups to the respective visible vibrations as a result of different orientation of the Cu_2 tetracarboxylate clusters with respect to the metal surface. S: symmetric vibration, A: asymmetric vibration.

These factors need to show up in the respective equation:

$$f_{IR} = (i_A * \chi_S * 4) / (i_S * \chi_A * 2) \quad \text{Eq. 8}$$

All the other contributions have their TDM oriented parallel to the surface and therefore are silent:

$$\chi_A + \chi_S = 1 \quad \text{Eq. 9}$$

Taken together, the above equations give χ_A, the proportion of upright oriented Cu clusters, which equals the proportion of [001] oriented crystals:

$$\chi_A = \frac{1}{1 + \frac{i_S}{2 \times i_A} \times \frac{I_A}{I_S}} \quad \text{Eq. 10}$$

The proportion χ_B can be calculated accordingly.

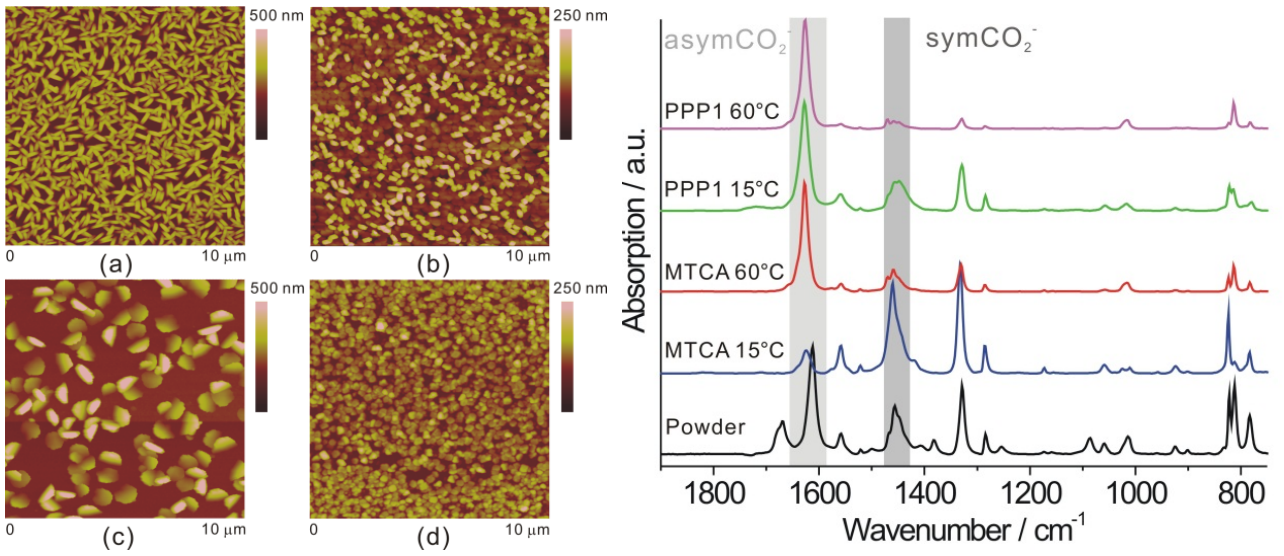

Figure S10. Temperature dependency in the $[Zn_2(adc)_2(dabco)]$ SURMOF system. When deposited on MTCA surfaces, the desired [110] orientation can only be obtained at 15 °C (a), while at 60 °C a mixture of orientations is obtained (b).The inverse effect can be observed at the PPP1 surface ((c): 15 °C, mixture of orientations (d): 60 °C, the desired [001] orientation). Note that the morphology in (c) differs from the one observed for the $[Cu_2(F_4bdc)_2(dabco)]$ system under the same conditions. The orientational order/disorder can be deduced from the IRRA spectra given on the right side.

References:

(1) Raiber, K.; Terfort, A.; Benndorf, C.; Krings, N.; Strehblow, H. H. *Surf. Sci.* **2005,** *595*, 56-63.

(2) Schüpbach, B.; Terfort, A. *Org. Biomol. Chem.* **2010,** *8*, 3522-3562.

(3) Himmel, H. J.; Terfort, A.; Wöll, C. *J. Am. Chem. Soc.* **1998,** *120*, 12069-12074.

(4) Chun, H.; Dybtsev, D. N.; Kim, H.; Kim, K. *Chem. Eur. J.* **2005,** *11*, 3521-3529.

(5) Gaussian 09, Revision A.02, Frisch, M. J.; Trucks, G. W.; Schlegel, H. B.; Scuseria, G. E.; Robb, M. A.; Cheeseman, J. R.; Scalmani, G.; Barone, V.; Mennucci, B.; Petersson, G. A.; Nakatsuji, H.; Caricato, M.; Li, X.; Hratchian, H. P.; Izmaylov, A. F.; Bloino, J.; Zheng, G.; Sonnenberg, J. L.; Hada, M.; Ehara, M.; Toyota, K.; Fukuda, R.; Hasegawa, J.; Ishida, M.; Nakajima, T.; Honda, Y.; Kitao, O.; Nakai, H.; Vreven, T.; Montgomery, J. A.; Jr.; Peralta, J. E.; Ogliaro, F.; Bearpark, M.; Heyd, J. J.; Brothers, E.; Kudin, K. N.; Staroverov, V. N.; Kobayashi, R.; Normand, J.; Raghavachari, K.; Rendell, A.; Burant, J. C.; Iyengar, S. S.; Tomasi, J.; Cossi, M.; Rega, N.; Millam, J. M.; Klene, M.; Knox, J. E.; Cross, J. B.;

Bakken, V.; Adamo, C.; Jaramillo, J.; Gomperts, R.; Stratmann, R. E.; Yazyev, O.; Austin, A. J.; Cammi, R.; Pomelli, C.; Ochterski, J. W.; Martin, R. L.; Morokuma, K.; Zakrzewski, V. G.; Voth, G. A.; Salvador, P.; Dannenberg, J. J.; Dapprich, S.; Daniels, A. D.; Farkas, O.; Foresman, J. B.; Ortiz, J. V.; Cioslowski, J. and Fox, D. J. Gaussian, Inc., Wallingford CT, 2009.

(6) Mathey, Y.; Gies, D. R.; Shriver, D. F. *Inorg. Chem.* **1982**, *21*, 3409-3413.

(7) Perdew, J. P.; Burke, K.; Ernzerhof, M. *Phys. Rev. Lett.* **1996**, *77*, 3865.

(8) a) Schaefer, A.; Horn, H.; Ahlrichs, R. *J. Chem. Phys.* **1992**, *97*, 2571. b) Weigend, F.; Ahlrichs, R. *Phys. Chem. Chem. Phys*., **2005**, *7*, 3297.

(9) Neese, F. ORCA - An ab initio, DFT and semiempirical SCF-MO package, (v. 2.8), Universität Bonn, Bonn, Germany, 2010.

(10) (a) Becke, A. D. *J. Chem. Phys.* **1993**, *98*, 5648; (b) Stephens, P. J.; Devlin, F. J.; Frisch, M. J.; Chabalowski, C. F. *J. Phys. Chem.* **1994**, *98*, 11623.

(11) Becke, A. D. *Phys. Rev. A* **1988**, *38*, 3098.

(12) (a) Lee, C.; Yang, W.; Parr, R. G. *Phys. Rev. B* **1988**, *37*, 785; (b) Miehlich, B.; Savin, A.; Stoll, H.; Preuss, H. *Chem. Phys. Lett.* **1989**, *157*, 200.

(13) Grimme, S.; Antony, J.; Ehrlich, S.; Krieg, H. *J. Chem. Phys.*, **2010**, *132*, 154104.

(14) Dolg, M.; Wedig, U.; Stoll, H.; Preuss, H. *J. Chem. Phys.* **1987**, *86*, 866.

(15) Martin, J. M. L.; Sundermann, A. *J. Chem. Phys.* **2001**, *114*, 3408..

(16) Sinnecker, S.; Rajendran, A.; Klamt, A.; Diedenhofen, M.; Neese, F. *J. Phys. Chem. A*, **2006**, *110*, 2235.